

MERLiN: Mixture Effect Recovery in Linear Networks

Sebastian Weichwald, Moritz Grosse-Wentrup, Arthur Gretton

Abstract—Causal inference concerns the identification of cause-effect relationships between variables. However, often only a linear combination of variables constitutes a meaningful causal variable. We propose to construct causal variables from non-causal variables such that the resulting statistical properties guarantee meaningful cause-effect relationships. Exploiting this novel idea, MERLiN is able to recover a causal variable from an observed linear mixture that is an effect of another given variable. We illustrate how to adapt the algorithm to a particular domain and how to incorporate a priori knowledge. Evaluation on both synthetic and experimental EEG data indicates MERLiN’s power to infer cause-effect relationships.

Index Terms—causal inference, causal variable construction, linear mixtures

I. INTRODUCTION

Causal inference requires causal variables. However, not always do the variables in a dataset specify the candidate causal relations. Images, for example, consist of microscopic variables (pixel colour values) while the identification of meaningful cause-effect relationships requires the construction of macroscopic causal variables (e.g. whether the image shows a magic wand) [1]. A similar problem often occurs whenever only a linear mixture of causal variables can be observed. In electroencephalography (EEG) studies, for example, what is measured at electrodes placed on the scalp is considered to be instantaneously and linearly superimposed electromagnetic activity of sources in the brain [2]. Standard causal inference methods would require that first all underlying causal variables are constructed –or rather recovered– from the observed mixture.

There exist a plethora of methods to construct macroscopic variables both from images and linear mixtures. However, prevailing methods to learn visual features [3]–[5] ignore the causal aspect and are fundamentally different from the recent and only work that demonstrates how visual *causal* features can be learned by a sequence of interventional experiments [1]. Likewise, methods to (re-)construct variables from linear mixtures commonly ignore the causal aspect and often rest on implausible assumptions. For instance, independent component analysis (ICA), commonly employed in the analysis of EEG data, rests on the assumption of mutually

independent sources [6]–[8]. One may argue that muscular or ocular artifacts are independent of the cortical sources and can be extracted via ICA [9], [10]. It seems implausible, though, that cortical sources are mutually independent. In fact, if they were mutually independent there would be no cause-effect relationships between them. Thus, it goes without saying that methods ignoring the causal aspect are incapacitated for the construction of meaningful causal variables.

Mixture Effect Recovery in Linear Networks (MERLiN) aims to construct a causal variable from a linear mixture without requiring multiple interventional experiments. The fundamental idea is to directly search for statistical in- and dependences that imply, under assumptions discussed below, a certain cause-effect relationship. In essence, given iid samples of a univariate randomised variable S , a univariate causal effect C_1 of S , and a multivariate variable F , MERLiN searches for a linear combination w such that $w^\top F$ is a causal effect of C_1 . This exemplifies the novel idea to construct causal variables such that the resulting statistical properties guarantee meaningful cause-effect relationships.

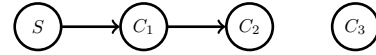


Fig. 1. Example graph.

As an illustration, consider the directed acyclic graph (DAG) shown in Figure 1. In this notation edges denote cause-effect relationships starting at the cause and pointing towards the effect. S denotes a randomised variable. We assume that only a linear mixture $F = A[C_1, C_2, C_3]^\top$ (A is a mixing matrix) of the causal variables C_1, C_2, C_3 can be observed and that $C_1 = v^\top F$. MERLiN’s goal is to recover from F an effect of C_1 , i.e. to find w such that $w^\top F$ is an effect of C_1 where $w^\top F = C_2$ is a possible solution.

We introduce the basic MERLiN $_{\Sigma-1}$ algorithm that can recover the sought-after causal variable when the cause-effect relationships are linear with additive Gaussian noise. Using our prime example, the analysis of EEG data, we illustrate how to adapt the algorithm to a particular domain and how to incorporate a priori knowledge. For stimulus-based neuroimaging studies, the MERLiN $_{\Sigma-1}^{bp}$ and MERLiN $_{\Sigma-1}^{b+}$ algorithms can establish a cause-effect relationship between brain state features that are observed only as part of a linear mixture. As such, MERLiN is able to provide insights into brain networks beyond those readily obtained from encoding and decoding models trained on pre-defined variables [11]. Furthermore, it employs the framework of Causal Bayesian Networks (CBNs) that has recently been pushed forward in the neuroimaging community [11]–[16] — the important advantage over methods based on information flow being that it yields testable

Sebastian Weichwald is with the Empirical Inference Department, Max Planck Institute for Intelligent Systems, Tübingen, Germany, and has been with the Centre for Computational Statistics and Machine Learning, University College London, London, United Kingdom, e-mail: sweichwald@tue.mpg.de.

Moritz Grosse-Wentrup is with the Empirical Inference Department, Max Planck Institute for Intelligent Systems, Tübingen, Germany, e-mail: moritzgw@tuebingen.mpg.de.

Arthur Gretton is with the Gatsby Computational Neuroscience Unit, Sainsbury Wellcome Centre, London, United Kingdom, e-mail: arthur.gretton@gmail.com.

predictions on the impact of interventions [17], [18].

MERLiN shows good performance both on synthetic and EEG data recorded during neurofeedback experiments. The Python/Matlab implementation for all presented algorithms is available on <https://github.com/sweichwald/MERLiN>.

II. METHODS

A. Causal Bayesian Networks

We briefly introduce the main aspects of Causal Bayesian Networks (CBNs). For an exhaustive treatment see [19], [20].

Definition 1 (Structural Equation Model). We define a *structural equation model* (SEM) \mathcal{S} as a set of equations $X_i = f_i(\mathbf{PA}_i, N_i)$, $i \in \mathbb{N}_{1:s}$ where the so-called noise variables are independently distributed according to $\mathbb{P}^{N_1, \dots, N_s} = \mathbb{P}^{N_1} \dots \mathbb{P}^{N_s}$. For $i \in \mathbb{N}_{1:s}$ the set $\mathbf{PA}_i \subseteq \{X_1, \dots, X_s\} \setminus X_i$ contains the so-called parents of X_i and f_i describes how X_i relates to the random variables in \mathbf{PA}_i and N_i . The induced joint distribution is denoted by $\mathbb{P}^{\mathcal{S}} \triangleq \mathbb{P}^{X_1, \dots, X_s}$.

Replacing at least one of the functions f_i , $i \in \mathbb{N}_{1:s}$ by a constant \spadesuit yields a new SEM. We say X_i has been intervened on, which is denoted by $\text{do}(X_i = \spadesuit)$, leads to the SEM $\mathcal{S}|\text{do}(X_i = \spadesuit)$, and induces the *interventional distribution* $\mathbb{P}^{\mathcal{S}|\text{do}(X_i = \spadesuit)} = \mathbb{P}^{X_1, \dots, X_s|\text{do}(X_i = \spadesuit)}$.

Definition 2 (Cause and Effect). X_i is a *cause* of X_j ($i, j \in \mathbb{N}_{1:s}$, $i \neq j$) wrt. a SEM \mathcal{S} iff there exists $\heartsuit \in \mathbb{R}$ such that $\mathbb{P}^{X_j|\text{do}(X_i = \heartsuit)} \neq \mathbb{P}^{X_j}$.¹ X_j is an *effect* of X_i iff X_i is a cause of X_j . Often the considered SEM \mathcal{S} is omitted if it is clear from the context.

For each SEM \mathcal{S} there is a corresponding graph $\mathcal{G}_{\mathcal{S}}(V, E)$ with $V = \{X_1, \dots, X_s\}$ and $E = \{(X_i, X_j) : X_i \in \mathbf{PA}_j, X_j \in V\}$ that has the random variables as nodes and directed edges pointing from parents to children. We employ the common assumption that this graph is acyclic, i.e. $\mathcal{G}_{\mathcal{S}}$ will always be a directed acyclic graph (DAG).

It is insightful to consider the following implication of Definition 2: If in $\mathcal{G}_{\mathcal{S}}$ there is no directed path from X_i to X_j , X_i is not a cause of X_j (wrt. \mathcal{S}). The following example shows that without further assumptions the converse is not true in general. We provide supportive graphical depictions in Figure 3.

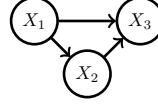
Example 3. Consider a SEM \mathcal{S} with structural equations and graph $\mathcal{G}_{\mathcal{S}}$ shown in Figure 2a and noise variables $(N_1, N_2, N_3) \sim \mathcal{N}(0, 1)^3$. In $\mathcal{G}_{\mathcal{S}}$ there is a directed path (in fact even a directed edge) from X_1 to X_3 while $\mathbb{P}^{X_3|\text{do}(X_1 = \heartsuit)} = \mathbb{P}^{X_3} = \mathbb{P}^{N_2 + N_3} = \mathcal{N}(0, 2)$ for all $\heartsuit \in \mathbb{R}$, i.e. X_1 is not a cause of X_3 wrt. \mathcal{S} (cf. Figure 2b).

Observe that $\mathbb{P}^{X_3|\text{do}(X_2 = \heartsuit)} = \mathcal{N}(\heartsuit, 2) \neq \mathcal{N}(0, 2) = \mathbb{P}^{X_3}$ for $\heartsuit \neq 0$, i.e. X_2 is, as one may intuitively expect, a cause of X_3 wrt. \mathcal{S} (cf. Figure 2c). Likewise, X_3 indeed turns out not to be a cause of X_1 or X_2 as can be seen from Figure 2d.

So far a DAG $\mathcal{G}_{\mathcal{S}}$ simply depicts all parent-child relationships defined by the SEM \mathcal{S} . Missing directed paths indicate

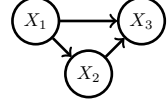
¹ $\mathbb{P}^{X_j|\text{do}(X_i = \heartsuit)}$ and \mathbb{P}^{X_j} denote the marginal distributions of X_j corresponding to $\mathbb{P}^{\mathcal{S}|\text{do}(X_i = \heartsuit)}$ and $\mathbb{P}^{\mathcal{S}}$ respectively.

$$\begin{aligned} X_1 &= N_1 \\ X_2 &= -X_1 + N_2 \\ X_3 &= X_1 + X_2 + N_3 \end{aligned}$$



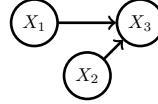
(a) SEM \mathcal{S} and graph $\mathcal{G}_{\mathcal{S}}$.

$$\begin{aligned} X_1 &= \heartsuit \\ X_2 &= -X_1 + N_2 \\ X_3 &= X_1 + X_2 + N_3 \end{aligned}$$



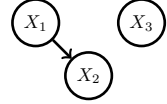
(b) SEM $\mathcal{S}|\text{do}(X_1 = \heartsuit)$ and graph $\mathcal{G}_{\mathcal{S}|\text{do}(X_1 = \heartsuit)}$.

$$\begin{aligned} X_1 &= N_1 \\ X_2 &= \heartsuit \\ X_3 &= X_1 + X_2 + N_3 \end{aligned}$$



(c) SEM $\mathcal{S}|\text{do}(X_2 = \heartsuit)$ and graph $\mathcal{G}_{\mathcal{S}|\text{do}(X_2 = \heartsuit)}$.

$$\begin{aligned} X_1 &= N_1 \\ X_2 &= -X_1 + N_2 \\ X_3 &= \heartsuit \end{aligned}$$



(d) SEM $\mathcal{S}|\text{do}(X_3 = \heartsuit)$ and graph $\mathcal{G}_{\mathcal{S}|\text{do}(X_3 = \heartsuit)}$.

Fig. 2. SEMs and graphs accompanying example 3.

missing cause-effect relationships. In order to specify the link between statistical independence (denoted by $\perp\!\!\!\perp$) wrt. the joint distribution $\mathbb{P}^{\mathcal{S}}$ and properties of the DAG $\mathcal{G}_{\mathcal{S}}$ (representing a SEM \mathcal{S}) we need the following definitions.

Definition 4 (d-separation). For a fixed graph \mathcal{G} disjoint sets of nodes A and B are *d-separated* by a third disjoint set C (denoted by $A \perp_{\text{d-sep}} B|C$) iff all pairs of nodes $a \in A$ and $b \in B$ are d-separated by C . A pair of nodes $a \neq b$ is d-separated by C iff every path between a and b is blocked by C . A path between nodes a and b is blocked by C iff there is an intermediate node z on the path such that (i) $z \in C$ and z is tail-to-tail ($\leftarrow z \rightarrow$) or head-to-tail ($\rightarrow z \rightarrow$), or (ii) z is head-to-head ($\rightarrow z \leftarrow$) and neither z nor any of its descendants is in C .

Definition 5 (Markov property). A distribution $\mathbb{P}^{X_1, \dots, X_s}$ satisfies the *global Markov property* wrt a graph \mathcal{G} if

$$A \perp_{\text{d-sep}} B|C \implies A \perp\!\!\!\perp B|C.$$

It satisfies the *local Markov property* wrt \mathcal{G} if each node is conditionally independent of its non-descendants given its parents. Both properties are equivalent if $\mathbb{P}^{X_1, \dots, X_s}$ has a density² (cf. [21, Theorem 3.27]); in this case we say $\mathbb{P}^{X_1, \dots, X_s}$ is *Markov* wrt \mathcal{G} .

Definition 6 (Faithfulness). $\mathbb{P}^{\mathcal{S}}$ generated by a SEM \mathcal{S} is said to be *faithful* wrt. $\mathcal{G}_{\mathcal{S}}$, if

$$A \perp_{\text{d-sep}} B|C \iff A \perp\!\!\!\perp B|C.$$

Conveniently the distribution $\mathbb{P}^{\mathcal{S}}$ generated by a SEM \mathcal{S} is Markov wrt. $\mathcal{G}_{\mathcal{S}}$ (cf. [20, Theorem 1.4.1] for a proof). Hence, if we assume faithfulness³ conditional independences and d-

²For simplicity we assume that distributions have a density wrt. some product measure throughout this text.

³Intuitively, this is saying that conditional independences are due to the causal structure and not accidents of parameter values [19, p. 9].

separation properties become equivalent

$$A \perp_{\text{d-sep}} B|C \iff A \perp B|C$$

Summing up, we have defined interventional causation in terms of SEMs and have seen how a SEM gives rise to a DAG. This DAG has two convenient features. Firstly, the DAG yields a visualisation that allows to easily grasp missing cause-effect relationships that correspond to missing directed paths. Secondly, assuming faithfulness d-separation properties of this DAG are equivalent to conditional independence properties of the joint distribution. Thus, conditional independences translate into causal statements, e.g. ‘a variable becomes independent of all its non-effects given its immediate causes’ or ‘cause and effect are marginally dependent’. Furthermore, the causal graph \mathcal{G}_S can be identified from conditional independences observed in \mathbb{P}^S — at least up to a so-called *Markov equivalence class*, the set of graphs that entail the same conditional independences [22].

B. Formal problem description

The terminology introduced in Section II-A allows to precisely state the problem as follows.

1) *Assumptions*: Let S and C_1, \dots, C_d denote (finitely many) real-valued random variables. We assume existence of a SEM S , potentially with additional unobserved variables h_1, \dots, h_l , that induces $\mathbb{P}^S = \mathbb{P}^{S, C_1, \dots, C_d, h_1, \dots, h_l}$. We refer to the corresponding graph \mathcal{G}_S as the *true causal graph* and call its nodes *causal variables*. We further assume that

- S affects C_2 indirectly via C_1 ,⁴
- \mathbb{P}^S is faithful wrt. \mathcal{G}_S ,
- there are no edges in \mathcal{G}_S pointing into S .

In an experimental setting the last condition is ensured by randomising S .⁵ Figure 3 depicts an example of how \mathcal{G}_S might look like.

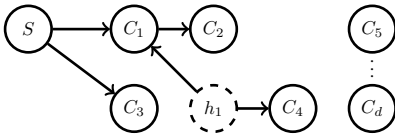


Fig. 3. Example graph where h_1 is a hidden variable.

2) Given data:

- m iid⁶ samples $\mathbf{S} = [s_1, \dots, s_m]^\top$ of S and $\mathbf{F} = [f_{i,j}]_{i=1:m, j=1:d'}$ of F where $F \triangleq [F_1, \dots, F_{d'}]^\top = \mathbf{A}\mathbf{C}$ is the observed linear mixture of the causal variables $\mathbf{C} \triangleq [C_1, \dots, C_d]^\top$ and $\mathbf{A} \in \mathbb{R}^{d' \times d}$ denotes the mixing matrix
- $\mathbf{v} \in \mathbb{R}^{d'}$ such that $C_1 = \mathbf{v}^\top \mathbf{F}$

⁴By saying a variable X causes Z indirectly via Y we imply (a) existence of a path $X \rightarrow Y \rightarrow Z$, and (b) that there is no path $X \rightarrow Z$ without Y on it (this also excludes the edge $X \rightarrow Z$).

⁵Randomisation corresponds to an intervention: the structural equation of S is replaced by $S = N_1$ where N_1 is an independent randomisation variable, e.g. assigning placebo or treatment according to an independent Bernoulli variable.

⁶independent and identically distributed

3) *Desired output*: Find $\mathbf{w} \in \mathbb{R}^{d'}$ such that $aC_i = \mathbf{w}^\top \mathbf{F}$ where C_i is an effect of C_1 ($i \in \mathbb{N}_{2:d}, a \in \mathbb{R} \setminus \{0\}$). For example, recovery of the causal variable C_2 is a valid solution.

C. MERLiN's strategy

We are given that there exists at least one causal variable C_2 that is indirectly affected by S via C_1 . However, we only have access to samples of the linear mixture F and samples of S . Note the following properties of C_2 :

- Since \mathbb{P}^S is Markov wrt. \mathcal{G}_S it follows that $C_2 \perp S|C_1$.
- Since \mathbb{P}^S is faithful wrt. \mathcal{G}_S it follows that $C_2 \not\perp C_1$ (and $C_2 \not\perp S$).

Conversely, we can derive the following sufficient conditions for a causal variable to be indirectly affected by S via C_1 .

Claim 7. Given the assumptions in Section II-B1 and a causal variable Y . If $Y \perp S|C_1$ and $Y \not\perp C_1$, then S indirectly affects Y via C_1 . In particular, a path $C_1 \rightarrow Y$ exists.

Proof: From $Y \not\perp C_1$ and \mathbb{P}^S being Markov wrt. \mathcal{G}_S it follows that Y and C_1 are not d-separated in \mathcal{G}_S by the empty set. In \mathcal{G}_S there must be at least one path $C_1 \rightarrow Y$, $C_1 \leftarrow Y$ or $C_1 \leftarrow X \rightarrow Y$ for some node X . By assumption C_1 is affected by S , i.e. we have $S \rightarrow C_1$ in \mathcal{G}_S . Hence, in \mathcal{G}_S there must be at least one path $S \rightarrow C_1 \rightarrow Y$, $S \rightarrow C_1 \leftarrow Y$ or $S \rightarrow C_1 \leftarrow X \rightarrow Y$ for some node X . Under the assumption of faithfulness, the latter two cases contradict $Y \perp S|C_1$. Hence, in \mathcal{G}_S at least one path $S \rightarrow C_1 \rightarrow Y$ exists.

From $Y \perp S|C_1$ and \mathbb{P}^S being faithful wrt. \mathcal{G}_S it follows that Y and S are d-separated in \mathcal{G}_S by C_1 . That is, given C_1 every path between S and Y is blocked. In particular, in \mathcal{G}_S there is no edge $S \rightarrow Y$ and no path $S \rightarrow Y$ without C_1 on it. Hence, Y is indeed indirectly affected by S via C_1 . ■

This leads to our general idea on how to find a linear combination that recovers a causal effect of C_1 . If MERLiN finds $\mathbf{w} \in \mathbb{R}^{d'}$ such that

- (a) $\mathbf{w}^\top \mathbf{F} \not\perp C_1$, and
- (b) $\mathbf{w}^\top \mathbf{F} \perp S|C_1$

then we have identified a candidate causal effect of C_1 . Ideally and under assumptions discussed below, optimising \mathbf{w} wrt. these statistical properties will indeed recover a *causal variable*, i.e. $\mathbf{w}^\top \mathbf{F} = aC_i$ ($i \in \mathbb{N}_{2:d}, a \in \mathbb{R} \setminus \{0\}$), that is an effect of C_1 .

D. Mixing assumptions

There may not exist a solution to MERLiN's problem if \mathbf{A} has rank less than d .⁷ Hence, assume that \mathbf{A} has rank d and, for simplicity, that \mathbf{A} is a square $d \times d$ matrix. This guarantees existence of a solution: if the mixing matrix \mathbf{A} is invertible a solution to the problem is to recover C_2 via $\mathbf{w} = \mathbf{A}_{2,1:d}^{-1}$. However, if we only assume \mathbf{A} to be invertible MERLiN may

⁷Note that \mathbf{A} being at least rank d is not a necessary condition, i.e. an effect of C_1 may be recoverable even in cases where \mathbf{A} has rank less than d . As an example consider the case where C_2 is an effect of C_1 and $\mathbf{A} = [\mathbf{I}_{d \times 2}, \mathbf{0}_{d \times (d-2)}]$. The aim of this section, however, is to derive a sufficient condition.

not be able to recover (a multiple of) a causal variable C_i from the sought-after statistical properties alone. This is the case even if C_2 is the only effect of C_1 and C_3, \dots, C_d are not effects of C_1 . The following (counter-)example demonstrates the problem that adding C_1 onto independent variables results in a variable that has the sought-after statistical properties but is not a causal variable.⁸

Example 8. Consider $S \rightarrow C_1 \rightarrow C_2 \leftarrow C_3$ is the true causal graph, where the gap indicates that C_3 is independent of all the other variables. Assume all variables have non-zero variance and that $C_2 = C_1 + N_2$ where N_2 acts as independent additive noise (again with non-zero variance). Let \mathbf{A} be an invertible real 3×3 matrix. For $F = \mathbf{A}C = \mathbf{A}[C_1, C_2, C_3]^\top$ and for all $a, b, c \in \mathbb{R}$, $a \neq -b$ we have $(a\mathbf{A}_{1,1:d}^{-1} + b\mathbf{A}_{2,1:d}^{-1} + c\mathbf{A}_{3,1:d}^{-1})F = (a+b)C_1 + bN_2 + cC_3 \triangleq Y_{a,b,c}$. Furthermore, the sought-after statistical properties hold true, i.e. $Y_{a,b,c} \not\perp\!\!\!\perp C_1$ and $Y_{a,b,c} \perp\!\!\!\perp S|C_1$ (cf. Claim 7).

Without imposing further constraints we can always add C_1 onto independent variables in order to obtain a variable that has the sought-after statistical properties, e.g. $Y_{1,0,1} = C_1 + C_3$. Likewise, adding C_1 onto an effect does not alter these properties, e.g. $Y_{1,1,0} = C_1 + C_2$. Hence, a valid solution to our problem (one for which $\mathbf{w}^\top F = aC_i$, $i \in \mathbb{N}_{2:d}$, $a \in \mathbb{R} \setminus \{0\}$) is not identifiable from the marginal dependence and conditional independence properties alone. The problem is inherently unidentifiable.

One way to mitigate this situation is to restrict search to the orthogonal complement \mathbf{v}_\perp of \mathbf{v} . This way, the signal of C_1 in the linear mixture F is attenuated. In particular, if the mixing matrix \mathbf{A} is orthogonal restricting search to \mathbf{v}_\perp amounts to complete removal of C_1 's signal from F . It is no longer possible to add in arbitrary multiples of C_1 to introduce (or strengthen) the sought-after dependence. While adding independent variables onto effects is still possible (e.g. consider $Y_{0,1,1} = C_2 + C_3$ in above example), it will be counter-acted by setting up the objective function accordingly — roughly speaking, as we ‘maximise dependence’ adding in independent variables, thus acting as noise, will be suppressed.

Henceforth, we assume that \mathbf{A} is an orthogonal $d \times d$ matrix and restrict search to \mathbf{v}_\perp .

E. Gradient ascent on the Stiefel manifold

MERLiN only aims at finding a causal variable up to a scaling factor. Hence, we will optimise objective functions over the unit-sphere $O^{n-1} \triangleq \{\mathbf{x} \in \mathbb{R}^n : \|\mathbf{x}\| = 1\}$. For generality we view the sphere as a special case of the Stiefel manifold $V_{n \times p} \triangleq \{\mathbf{M} \in \mathbb{R}^{n \times p} : \mathbf{M}^\top \mathbf{M} = \mathbf{I}_{p \times p}\}$ ($p \leq n$) for $p = 1$. By performing gradient ascent directly on the Stiefel manifold we avoid taking free gradient ascent steps and projecting back onto $V_{n \times p}$. Steps will be taken along a geodesic, i.e. the shortest path between two points on this manifold. We state the update rule that accomplishes this while

⁸The example also demonstrates how additive noise poses a problem for ICA. Decomposing $C_2 = C_1 + N_2$ into independent ‘sources’ C_1 and N_2 only correctly recovers one underlying source while the causal variable C_2 is incorrectly dismembered.

the reader is referred to [23] for more details. Given a current position $\mathbf{V} \in V_{n \times p}$, the free gradient $\mathbf{G} \in \mathbb{R}^{n \times p}$ at \mathbf{V} of an objective function, and a step size t the gradient ascent update on the Stiefel manifold is

$$\pi_{\text{Stiefel}}(\mathbf{V}, \mathbf{G}, t) \triangleq [\mathbf{V}, \mathbf{V}_\perp] \exp \left[t \begin{bmatrix} \mathbf{V}^\top \mathbf{G} - \mathbf{G}^\top \mathbf{V} & -\mathbf{G}^\top \mathbf{V}_\perp \\ \mathbf{V}_\perp^\top \mathbf{G} & \mathbf{0}_{(n-p) \times (n-p)} \end{bmatrix} \right] \mathbf{I}_{n \times p}.$$

The Stiefel gradient ascent algorithm used in this work is summarised in Algorithm 1. The gradients required in this work can readily be obtained via automatic differentiation (using e.g. theano for Python [24], [25]). Note that no line search techniques like Golden section search are employed since the number of local maxima on a line segment is unknown for the considered objective functions.

Algorithm 1 Stiefel gradient ascent.

Input: cost function $f : V_{n \times 1} \rightarrow \mathbb{R}$ its gradient $g : V_{n \times 1} \rightarrow V_{n \times 1}$, initial point \mathbf{w}_0

Procedure:

- for t from 1 to $T = 500$
 - set $\lambda := 1$
 - half λ while $f(\pi_{\text{Stiefel}}(\mathbf{w}_{t-1}, g(\mathbf{w}_{t-1}), \lambda)) < f(\mathbf{w}_{t-1})$
 - set $\mathbf{w}_t := \pi_{\text{Stiefel}}(\mathbf{w}_{t-1}, g(\mathbf{w}_{t-1}), \lambda)$
 - if $|f(\mathbf{w}_{t-1}) - f(\mathbf{w}_t)| < 10^{-16}$ set $T := t$ and stop

Output: \mathbf{w}_T and $f(\mathbf{w}_T)$

F. MERLiN _{Σ^{-1}} : precision matrix magic

MERLiN is now prepared to tackle the case of linear relationships with additive Gaussian noise. Here, zero entries in the precision matrix imply missing edges in the graph [21]. Hence, if Y is an effect of C_1 the precision matrix of the three variables S, C_1 and Y is of the form

$$\Sigma^{-1} \triangleq \Sigma_{S, C_1, Y}^{-1} = \begin{bmatrix} \star & \star & 0 \\ \star & \star & \star \\ 0 & \star & \star \end{bmatrix}$$

where stars indicate non-zero entries (here we assumed $d \leq m$ and invertibility). This implies the partial correlations $\rho_{Y, C_1 | S} = \star$ and $\rho_{Y, S | C_1} = 0$ which, in the Gaussian case, amount to the conditional (in-)dependencies $Y \not\perp\!\!\!\perp C_1 | S$ and $Y \perp\!\!\!\perp S | C_1$ [26]. Note that conditioning on S cannot unblock a path that was blocked before as there are no edges pointing into S , conversely $Y \not\perp\!\!\!\perp C_1 | S \implies Y \not\perp\!\!\!\perp C_1$.

Exploiting this link, the precision matrix based MERLiN _{Σ^{-1}} algorithm (cf. Algorithm 2) implements the general idea of optimising marginal dependence and conditional independence by maximising the objective function⁹

$$f(\mathbf{w}) = \left| \left(\hat{\Sigma}_{\mathbf{w}}^{-1} \right)_{2,3} \right| - \left| \left(\hat{\Sigma}_{\mathbf{w}}^{-1} \right)_{1,3} \right|$$

where $\hat{\Sigma}_{\mathbf{w}}^{-1} \triangleq \hat{\Sigma}_{S, C_1, \mathbf{w}^\top F}^{-1}$. Optimisation is accomplished by gradient ascent over the Stiefel manifold $V_{(d-1) \times 1}$ which is obtained by projecting \mathbf{F} onto the orthogonal complement \mathbf{v}_\perp .

⁹For numerical reasons one might want to use the approximation $\sqrt{\cdot + \epsilon} \approx |\cdot|$ for small $0 < \epsilon \in \mathbb{R}$ to ensure that f is differentiable everywhere.

Algorithm 2 MERLiN $_{\Sigma^{-1}}$ **Input:** $S \in \mathbb{R}^{m \times 1}$, $F \in \mathbb{R}^{d \times m}$, $v \in \mathbb{R}^{d \times 1}$ **Procedure:**

- set $C := F^\top v$ and $F := P(v)F \in \mathbb{R}^{(d-1) \times m}$
- define the objective function for $w \in O^{d-2}$ as

$$f(w) = \left| \left(\hat{\Sigma}_w^{-1} \right)_{2,3} \right| - \left| \left(\hat{\Sigma}_w^{-1} \right)_{1,3} \right|$$

where the empirical precision matrix is

$$\hat{\Sigma}_w^{-1} = \left(\frac{1}{m-1} [S, C, F^\top w]^\top H_m [S, C, F^\top w] \right)^{-1}$$

- obtain the gradient $g : O^{d-2} \rightarrow O^{d-2}$ of f via automatic differentiation
- set $w_0 \in O^{d-2}$ randomly
- run Stiefel gradient ascent (cf. Algorithm 1) for f, g, w_0 to obtain w_T

Output: $w = P(v)^\top w_T \in O^{d-1}$ **Definitions:**

- $P(v)$ is the $(d-1) \times d$ orthonormal matrix that accomplishes projection onto the orthogonal complement v_\perp
- $H_m = I_{m \times m} - \frac{1}{m} \mathbf{1}_{m \times m}$ is the $m \times m$ centering matrix

G. MERLiN $_{\Sigma^{-1}}^{bp}$: adaption to EEG data

We consider EEG trial-data of the form $\tilde{F} \in \mathbb{R}^{d \times m \times n}$ where d denotes the number of electrodes, m the number of trials, and n the length of the time series $\tilde{F}_{i,j,1:n}$ for each electrode $i \in \mathbb{N}_{1:d}$ and each sample $j \in \mathbb{N}_{1:m}$. Analyses of EEG data commonly focus on trial-averaged log-bandpower in a particular frequency band. Accordingly, we aim at identifying a linear combination $w \in \mathbb{R}^{d \times 1}$ such that the log-bandpower of the resulting one-dimensional trial signals $w^\top \tilde{F}_{1:d,j,1:n}$ is a causal effect of the log-bandpower of the one-dimensional trial signals $v^\top \tilde{F}_{1:d,j,1:n}$. However, since the two operations of computing the log-bandpower (after windowing) and taking a linear combination do not commute, we cannot compute the trial-averaged log-bandpower for each channel first and then apply the standard precision matrix based MERLiN $_{\Sigma^{-1}}$ algorithm. Instead, MERLiN $_{\Sigma^{-1}}^{bp}$ has been adapted to the analysis of EEG data by switching in the the log-bandpower computation.

To simplify the optimisation loop we exploit the fact that applying a Hanning window¹⁰ and the FFT to each channels' signal commutes with taking a linear combination of the windowed and Fourier transformed time series. Note that averaging of the log-moduli ($\log(|\cdot|)$) of the Fourier coefficients does not commute with taking a linear combination. Hence, windowing and computing the FFT is done in a separate preprocessing step (cf. Algorithm 3), while the trial-averaged bandpower is computed within the optimisation loop after taking the linear combination. Implementation details for the bandpower and precision matrix based MERLiN $_{\Sigma^{-1}}^{bp}$

¹⁰We apply a Hanning window in order to keep the feature computation in line with [16].

algorithm are described in Algorithm 4. Note, that to ease implementation we treat complex numbers as two-dimensional vector space over the reals.

Algorithm 3 Preprocessing for bp algorithm.**Input:** $S \in \mathbb{R}^{m \times 1}$, $\tilde{F} \in \mathbb{R}^{d \times m \times n}$, $v \in \mathbb{R}^{d \times 1}$, the sampling frequency f_s , and the desired frequency range defined by ω_1 and ω_2 **Procedure:**

- set $a := \lfloor \frac{\omega_1 n}{f_s} \rfloor$, $b := \lfloor \frac{\omega_2 n}{f_s} \rfloor$, and $n' := b - a + 1$
- for i from 1 to d , for j from 1 to m
 - center, apply Hanning window and compute FFT, i.e. treat $\tilde{F}_{i,j,1:n}$ as a column vector and set $\tilde{F}_{i,j,1:n} := TW H_n \tilde{F}_{i,j,1:n}$
- extract relevant Fourier coefficients corresponding to v , i.e. set

$$V^{\text{Im}} := \text{Im} \left(v^\top \tilde{F}_{1:d,j,a:b} \right)_{j=1:m} \in \mathbb{R}^{m \times n'}$$

$$V^{\text{Re}} := \text{Re} \left(v^\top \tilde{F}_{1:d,j,a:b} \right)_{j=1:m} \in \mathbb{R}^{m \times n'}$$

- remove direction v from \tilde{F} , i.e. for j from 1 to m set

$$F_{1:d,j,1:n'}^{\text{Im}} := \text{Im} \left(R(v) \tilde{F}_{1:d,j,a:b} \right) \in \mathbb{R}^{d \times n'}$$

$$F_{1:d,j,1:n'}^{\text{Re}} := \text{Re} \left(R(v) \tilde{F}_{1:d,j,a:b} \right) \in \mathbb{R}^{d \times n'}$$

such that $F^{\text{Im}}, F^{\text{Re}} \in \mathbb{R}^{d \times m \times n'}$ **Output:** $V^{\text{Im}}, V^{\text{Re}} \in \mathbb{R}^{m \times n'}$ and $F^{\text{Im}}, F^{\text{Re}} \in \mathbb{R}^{d \times m \times n'}$ **Definitions:**

- $H_n = I_{n \times n} - \frac{1}{n} \mathbf{1}_{n \times n}$ is the $n \times n$ centering matrix
- $W = \left[\frac{1}{2} \left(1 - \cos \frac{2\pi k}{n-1} \right) \right]_{k,l=1:n}$ is the $n \times n$ Hanning window matrix
- $T = [\exp(-i2\pi k \frac{l}{n})]_{k,l=1:n}$ is the $n \times n$ FFT matrix
- $R(v) = P(v)^\top P(v)$ is the $d \times d$ matrix that removes the direction v
- $P(v)$ is the $(d-1) \times d$ orthonormal matrix that accomplishes projection onto the orthogonal complement v_\perp

Algorithm 4 MERLiN $_{\Sigma^{-1}}^{bp}$

Refer to Algorithm 5 and instead use the objective function

$$f(w) = \left| \left(\hat{\Sigma}_w^{-1} \right)_{2,3} \right| - \left| \left(\hat{\Sigma}_w^{-1} \right)_{1,3} \right|$$

H. MERLiN $_{\Sigma^{-1}}^{bp+}$: incorporating a priori knowledge

A cortical source projects into more than one EEG electrode. In general, these volume conduction artifacts might lead to wrong conclusions about interactions between sources [27]. Imaginary coherency, as introduced in [28], may help to differentiate volume conduction artifacts from interactions between cortical sources. To briefly recap the rationale, employ the common assumption that the signals measured at the EEG

electrodes have no time-lag to the cortical signals [29]. The coherency at a certain frequency of two time series X and Y with Fourier coefficients $x(j), y(j), j \in \mathbb{N}_{1:n}$ is defined as

$$\text{coh}_{X,Y}(j) = \frac{\mathbb{E}[x(j)y^*(j)]}{\sqrt{\mathbb{E}[x(j)x^*(j)]\mathbb{E}[y(j)y^*(j)]}}$$

where $*$ denotes complex conjugation. Next consider the coherency of X and $Y + X$

$$\text{coh}_{X,Y+X} = \frac{\mathbb{E}[x(j)y^*(j)] + \mathbb{E}[x(j)x^*(j)]}{\sqrt{\mathbb{E}[x(j)x^*(j)]\mathbb{E}[(y(j)+x(j))(y^*(j)+x^*(j))]}}$$

and observe that $\mathbb{E}[x(j), x^*(j)]$ is real. This shows that non-zero imaginary coherency $\text{icoh}_{X,Y}(j) \triangleq \text{Im}(\text{coh}_{X,Y}(j))$ cannot be due to volume conduction and indicates time-lagged interaction between sources.¹¹

This a priori knowledge is incorporated in MERLiN^{bp+} _{Σ^{-1}} by adapting the objective function to be

$$f(\mathbf{w}) = \left| \sum_{j=1}^{n'} \text{icoh}(j) \right| \cdot \left| \left(\widehat{\Sigma}_{\mathbf{w}}^{-1} \right)_{2,3} \right| - \left| \left(\widehat{\Sigma}_{\mathbf{w}}^{-1} \right)_{1,3} \right|$$

where $\widehat{\Sigma}_{\mathbf{w}}^{-1}$ denotes the empirical precision matrix of the log-bandpower features after taking the linear combination \mathbf{w} and $\text{icoh}(j)$ denotes the imaginary coherency between the signals corresponding to \mathbf{v} and \mathbf{w} estimated as average over all trials (cf. Algorithm 5 for details). While there are several ways of setting up the objective function we have chosen this multiplicative set-up as it quite naturally captures the following idea: whenever we find the resulting bandpower to be affected by C_1 we also want to ensure that this is not just an artifact due to volume conduction. Note that this extension may also help disentangle true cortical sources, i.e. the causal variables, since a mixture of affected sources that have different time-lags and hence result in lower imaginary coherency is being avoided.

III. EXPERIMENTS ON SYNTHETIC DATA

A. Data description

$\mathcal{D}_T^{d \times m}(a, b)$ denotes the synthetic dataset that is generated by Algorithm 6. It consists of samples of an orthogonal linear mixture of underlying causal variables that follow the causal graph shown in Figure 3. The link between C_1 and C_2 becomes noisier for higher values of a , i.e. $\text{corr}(C_1, C_2)^2 = 2 + b^2 / (2 + b^2 + a^2)$. The parameter b adjusts the severeness of hidden confounding between C_1 and C_4 . Note also that the link between S and C_2 is weaker for higher values of b , i.e. $\text{corr}(S, C_2)^2 = 1 / (2 + b^2 + a^2)$.

By $\mathcal{T}\mathcal{D}_T^{d \times m \times n}(a, b)$ we denote a dataset that is generated from $\mathcal{D}_T^{d \times m}(a, b)$ with fixed mixing matrix $\mathbf{A} = \mathbf{I}_{d \times d}$ as follows. While $\mathbf{S}, \mathbf{v}, \mathbf{w}_{G0}$ remain unchanged the $d \times m$ matrix \mathbf{F} is replaced by a $d \times m \times n$ tensor $\tilde{\mathbf{F}}$ that consists of dm chunks of randomly chosen real EEG signals of length n . Each signal $\tilde{\mathbf{F}}_{i,j,1:n}$ is modified such that the log-bandpower in the desired frequency band equals $\mathbf{F}_{i,j}$. This data was used to sanity check the implementation of MERLiN^{bp} _{Σ^{-1}} .

¹¹Here we exploit the assumption of instantaneous mixing mentioned above.

Algorithm 5 MERLiN^{bp+} _{Σ^{-1}}

Input: $\mathbf{S} \in \mathbb{R}^{m \times 1}, \tilde{\mathbf{F}} \in \mathbb{R}^{d \times m \times n}, \mathbf{v} \in \mathbb{R}^{d \times 1}$, the sampling frequency f_s , and the desired frequency range defined by ω_1 and ω_2

Procedure:

- obtain $\mathbf{V}^{\text{Im}}, \mathbf{V}^{\text{Re}} \in \mathbb{R}^{m \times n'}$ and $\mathbf{F}^{\text{Im}}, \mathbf{F}^{\text{Re}} \in \mathbb{R}^{d \times m \times n'}$ via Algorithm 3
- set $\mathbf{C} := \left(\frac{1}{n'} \sum_{j=1}^{n'} \log_* \left(\frac{\sqrt{(\mathbf{V}_{i,j}^{\text{Im}})^2 + (\mathbf{V}_{i,j}^{\text{Re}})^2}}{n} \right) \right)_{i=1:m} \in \mathbb{R}^{m \times 1}$ (average log-bandpower per trial)
- define the objective function for $\mathbf{w} \in O^{d-1}$ as

$$f(\mathbf{w}) = \left| \sum_{j=1}^{n'} \text{icoh}(j) \right| \cdot \left| \left(\widehat{\Sigma}_{\mathbf{w}}^{-1} \right)_{2,3} \right| - \left| \left(\widehat{\Sigma}_{\mathbf{w}}^{-1} \right)_{1,3} \right|$$

where the empirical precision matrix is

$$\widehat{\Sigma}_{\mathbf{w}}^{-1} = \left(\frac{1}{m-1} [\mathbf{S}, \mathbf{C}, \mathbf{D}_{\mathbf{w}}]^\top \mathbf{H}_m [\mathbf{S}, \mathbf{C}, \mathbf{D}_{\mathbf{w}}] \right)^{-1},$$

the average log-bandpower per trial depending on \mathbf{w} is

$$\mathbf{D}_{\mathbf{w}} = \left(\frac{1}{n'} \sum_{j=1}^{n'} \log_* \left(\frac{\sqrt{(\mathbf{w}^\top \mathbf{F}_{1:d,i,j}^{\text{Im}})^2 + (\mathbf{w}^\top \mathbf{F}_{1:d,i,j}^{\text{Re}})^2}}{n} \right) \right)_{i=1:m} \in \mathbb{R}^{m \times 1},$$

and the imaginary coherency $\text{icoh}(j)$ for each frequency $j \in \mathbb{N}_{1:n'}$ equals

$$\frac{\langle \mathbf{V}_{i,j}^{\text{Im}}, \mathbf{w}^\top \mathbf{F}_{1:d,i,j}^{\text{Re}} - \mathbf{V}_{i,j}^{\text{Re}}, \mathbf{w}^\top \mathbf{F}_{1:d,i,j}^{\text{Im}} \rangle_{i=1:m}}{\sqrt{\langle (\mathbf{V}_{i,j}^{\text{Im}})^2 + (\mathbf{V}_{i,j}^{\text{Re}})^2 \rangle_{i=1:m} \langle (\mathbf{w}^\top \mathbf{F}_{1:d,i,j}^{\text{Im}})^2 + (\mathbf{w}^\top \mathbf{F}_{1:d,i,j}^{\text{Re}})^2 \rangle_{i=1:m}}}$$

- obtain the gradient $g : O^{d-1} \rightarrow O^{d-1}$ of f via automatic differentiation
- set $\mathbf{w}_0 \in O^{d-1}$ randomly
- run Stiefel gradient ascent (cf. Algorithm 1) for f, g, \mathbf{w}_0 to obtain \mathbf{w}_T

Output: $\mathbf{w}_T \in O^{d-1}$

Definitions:

- \log_* is the extended log function with $\log_*(x) = \log(x)$, $x > 0$ and $\log_*(0) = 0$
 - the notation $\langle \cdot \rangle_{i=1:m}$ denotes the empirical mean, i.e. $\langle a_i \rangle_{i=1:m} = \frac{1}{m} \sum_{i=1}^m a_i$
-

B. Assessing MERLiN's performance

We introduce two performance measures to assess MERLiN's performance on synthetic data with known ground truth \mathbf{w}_{G0} . Since a solution needs and in general can only be identified up to scaling, we only need to consider the $(d-1)$ -sphere $O^{d-1} = \{\mathbf{x} \in \mathbb{R}^d : \|\mathbf{x}\| = 1\}$. The closer a vector $\mathbf{w} \in O^{d-1}$ or its negation $-\mathbf{w}$ is to the ground truth $\mathbf{w}_{G0} \in O^{d-1}$ the better. This leads to the performance measure of **angular distance**

$$\text{andi}_{\mathbf{w}_{G0}}(\mathbf{w}) \triangleq \min(\angle(\mathbf{w}, \mathbf{w}_{G0}), \angle(-\mathbf{w}, \mathbf{w}_{G0})) \in [0, \pi/2]$$

Another viewpoint is to assess the quality of a found \mathbf{w} by the probability to obtain a vector that is closer to \mathbf{w}_{G0} if uniform randomly picking a vector on the $(d-1)$ -sphere. We

Algorithm 6 Generating the synthetic dataset $\mathcal{D}_T^{d \times m}(a, b)$.

Input: $d, m \in \mathbb{N}$, $a, b \in \mathbb{R}$, $T \in \{G, B\}$

Procedure:

- generate a random orthogonal^a $d \times d$ matrix \mathbf{A} by Gram-Schmidt orthonormalising a matrix with entries independently drawn from a standard normal distribution
- set $\mathbf{v}^\top := (\mathbf{A}^{-1})_{1,1:d} = (\mathbf{A}^\top)_{1,1:d}$
- set $\mathbf{w}_{G0}^\top := (\mathbf{A}^{-1})_{2,1:d} = (\mathbf{A}^\top)_{2,1:d}$
- generate independent mean parameters $\mu_1, \dots, \mu_d, \mu_{h_1}$ from $\mathcal{N}(0, 1)$
- generate m independent samples according to the following SEM

$$\begin{aligned} S &= N_0 \\ C_1 &= \mu_1 + N_1 + S + bh_1 \\ C_2 &= \mu_2 + aN_2 + C_1 \\ C_3 &= \mu_3 + N_3 + S \\ C_4 &= \mu_4 + N_4 + bh_1 \\ C_k &= \mu_k + N_k \quad (k \in \mathbb{N}_{5:d}) \end{aligned}$$

where $(N_1, \dots, N_d) \sim \mathcal{N}(0, 1)^d$, $h_1 \sim \mathcal{N}(\mu_{h_1}, 1)$, and $N_0 \sim \text{Unif}(\{-1, +1\})$ if $T = B$ or $S \sim \mathcal{N}(0, 1)$ if $T = G$

- arrange the m samples s_1, \dots, s_m of S in a column vector \mathbf{S}
- arrange each sample of (C_1, \dots, C_d) in a column vector and (pre-)multiply by \mathbf{A} to obtain the corresponding sample of (F_1, \dots, F_d)
- arrange the m samples of (F_1, \dots, F_d) as columns of a $d \times m$ matrix \mathbf{F}

Output: $\mathbf{S}, \mathbf{F}, \mathbf{v}, \mathbf{w}_{G0}$

^aSince we can ignore scaling, it is not a problem that we in fact generate an orthonormal matrix.

define the probability of a better vector as

$$\text{pobv}_{\mathbf{w}_{G0}}(\mathbf{w}) \triangleq \mathbb{P}[|\mathbf{w}_r \cdot \mathbf{w}_{G0}| > |\mathbf{w} \cdot \mathbf{w}_{G0}|]$$

where $\mathbf{w}_r \sim \text{Unif}(O^{d-1})$ and d is the dimension of the input vector. This quantity is obtained by dividing the area of the smallest hyperspherical cap centred at \mathbf{w}_{G0} that contains \mathbf{w} or $-\mathbf{w}$ by half the area of the $(d-1)$ -sphere. The former equals the area of the hyperspherical cap of height $h = 1 - |\mathbf{w} \cdot \mathbf{w}_{G0}|$, the latter equals the area of the hyperspherical cap of height $r = 1$. Exploiting the concise formulas for the area of a hyperspherical cap with radius r presented in [30] we obtain

$$\text{pobv}_{\mathbf{w}_{G0}}(\mathbf{w}) = I_{h(2-h)}\left(\frac{d-1}{2}, \frac{1}{2}\right)$$

where $h = 1 - |\mathbf{w} \cdot \mathbf{w}_{G0}|$ and $I_x(a, b)$ is the regularized incomplete beta function. It is interesting to note that $I_x(d-1/2, 1/2)$ is the cumulative distribution function of a $\text{Beta}(d-1/2, 1/2)$ distribution such that $|\mathbf{w}_r \cdot \mathbf{w}_{G0}|^2 \sim \text{Beta}(1/2, d-1/2)$.

For simplicity we drop the ground truth vector \mathbf{w}_{G0} from

the notation and simply assume that always the corresponding ground truth vector is considered. Both performance measures are related as in $\text{pobv}(\mathbf{w}) = 0$ iff $\text{andi}(\mathbf{w}) = 0$ and $\text{pobv}(\mathbf{w}) = 1$ iff $\text{andi}(\mathbf{w}) = \pi/2$. However, they capture somewhat complementary information: $\text{andi}(\mathbf{w})$ assesses how close the vector is in absolute terms, while $\text{pobv}(\mathbf{w})$ respects the fact that the problem becomes much harder in higher dimensions.

C. Experimental results

We applied the precision matrix based MERLiN $_{\Sigma^{-1}}$ algorithm (cf. Algorithm 2) to the synthetic datasets $\mathcal{D}_T^{d \times m}(a, b)$ described in Section III-A. The results of 100 runs¹² for different configurations of d, m, a, b are summarised as boxplots in Figures 4 and 5. Recall that the lower the values of $\text{pobv}_{\mathbf{w}_{G0}}(\mathbf{w})$ and $\text{andi}_{\mathbf{w}_{G0}}(\mathbf{w})$ the closer the found vector \mathbf{w} is to the ground truth \mathbf{w}_{G0} . We observe the following:

- The results for Gaussian ($T = G$) or binary ($T = B$; not shown here) variable S are indistinguishable.
- The performance is insensitive to the severity of hidden confounding which can be seen by comparing the plots row-wise for the different values of b . This behaviour is expected since $C_4 \not\propto S|C_1$.
- The performance decreases with increasing noise level, i.e. with increasing values of a . Note, that $a = 1$ corresponds to the case, where C_2 is a sum of C_1 and S both with variance 1.
- The problem becomes harder in higher dimensions resulting in worse performance. However, the results for $\text{pobv}_{\mathbf{w}_{G0}}(\mathbf{w})$ indicate that even if the found solution is not that close to \mathbf{w}_{G0} in an absolute sense ($\text{andi}_{\mathbf{w}_{G0}}(\mathbf{w})$) the solution is good in an probabilistic sense.
- More samples increase performance. Especially if the noise level a and the dimension d are not both high at the same time, MERLiN still achieves good performance on $m = 300$ samples (cf. e.g. the results for $a = 0.1$, $d = 100$ or $a = 1$, $d = 5$).

Sanity checks of MERLiN $_{\Sigma^{-1}}^{bp}$ on $\mathcal{TD}_T^{d \times m \times n}(a, b)$ showed similar trends for varying parameters T, d, m, a, b .

IV. EXPERIMENTS ON EEG DATA

A. Data description

We challenge MERLiN with EEG data recorded during a neurofeedback experiment [31].¹³ Subjects in this study were instructed in pseudo-randomised order to up- or down-regulate the amplitude of γ -oscillations (55–85 Hz) in the right superior parietal cortex (SPC). For the feedback the activity in the SPC was extracted by a linearly-constrained-minimum variance (LCMV) beamformer [32] that was trained on 5 min resting-state EEG data.

¹²For each run we create a new dataset. This is the case for all experiments on synthetic data. The performance measures $\text{andi}_{\mathbf{w}_{G0}}(\mathbf{w})$ and $\text{pobv}_{\mathbf{w}_{G0}}(\mathbf{w})$ are always considered wrt. the corresponding \mathbf{w}_{G0} of each dataset instance.

¹³Data was recorded at 121 active electrodes placed according to the extended 10–20 system at a sampling frequency of 500 Hz and converted to common average reference.

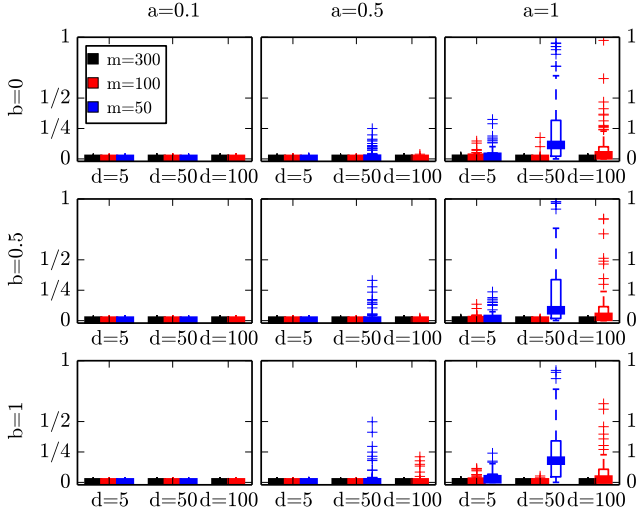


Fig. 4. The boxplots summarise the results of 100 experiments running $\text{CERLiM}_{\Sigma-1}$ on datasets $\mathcal{D}_T^{d \times m}(a, b)$ for $T = G$ (cf. Section III-A). The performance measure $\text{pobv}_{w_{G0}}(w)$ is shown on the y -axes and described in Section III-B (low values are good). The box for $d = 100, m = 50$ is missing since $\text{MERLiN}_{\Sigma-1}$ can only be applied if $d \leq m$.

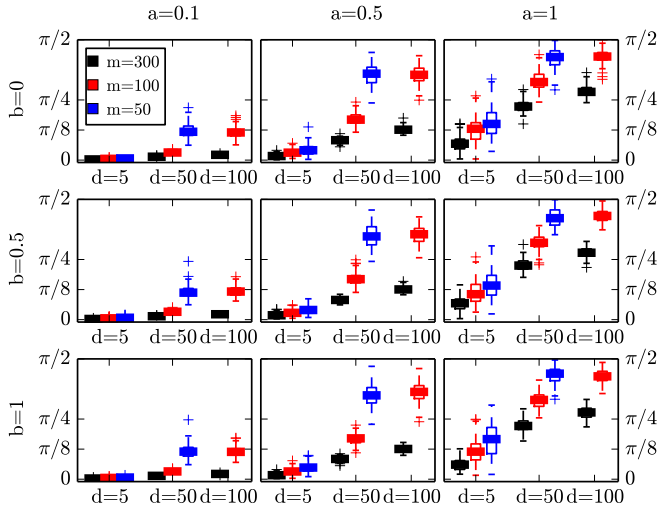


Fig. 5. The boxplots summarise the results of 100 experiments running $\text{CERLiM}_{\Sigma-1}$ on datasets $\mathcal{D}_T^{d \times m}(a, b)$ for $T = G$ (cf. Section III-A). The performance measure $\text{and}_{w_{G0}}(w)$ is shown on the y -axes and described in Section III-B (low values are good). The box for $d = 100, m = 50$ is missing since $\text{MERLiN}_{\Sigma-1}$ can only be applied if $d \leq m$.

Each recording session (3 subjects á 2 sessions referred to as S1R1, S1R2, S2R1, ...) consists of 60 trials á 60 seconds. The stimulus variable S is either $+1$ or -1 depending on whether the subject was instructed to up- or down-regulate γ -power in the SPC. Electromagnetic artifacts were attenuated as described in [31, Section 2.4.1] and the EEG data downsampled to 250 Hz. We are also given the spatial filter $v \in \mathbb{R}^{121 \times 1}$ for each session, i.e. the beamformer that was used to extract the feedback signal. Thus, the data of one session can be arranged as $S \in \{-1, +1\}^{60 \times 1}$, $v \in \mathbb{R}^{121 \times 1}$ and $\tilde{F} \in \mathbb{R}^{121 \times 60 \times 15000}$ where \tilde{F} contains the timeseries (of length 15000) for each channel and trial.

B. Assessing MERLiN's performance

MERLiN's performance on this data is assessed by comparing against results from an earlier exhaustive search approach. The hypothesis in [16] was that γ -oscillations in the SPC modulate γ -oscillations in the medial prefrontal cortex (MPC) and was derived from previous transcranial magnetic stimulation studies [33]. In order to test this hypothesis the signal of $K \triangleq 15028$ dipoles across the cortical surface was extracted using a LCMV beamformer and a three-shell spherical head model [34]. The SCI algorithm was used to assess for every dipole whether its γ -log-bandpower is a causal effect of the γ -log-bandpower in the SPC. This analysis confirmed the MPC as a causal effect of the SPC (cf. Figure 6).

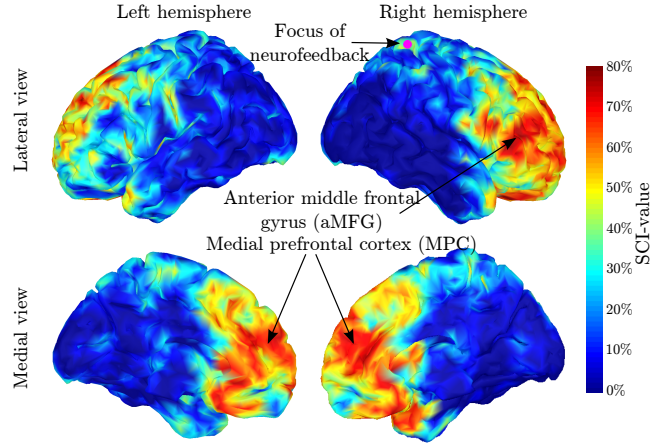


Fig. 6. Figure taken from [16]. The neurofeedback target area in the right SPC is indicated by a pink circle. The SCI value denotes the percentage of dipoles within a radius of 7 mm that were found to be modulated by the SPC. From these results, the authors inferred the primary targets of the right SPC to be the MPC and additionally the right aMFG.

To allow comparison against these results we derive a vector $g \in \mathbb{R}^{K \times 1}$ that represents the involvement of each cortical dipole in the signal identified by $\text{MERLiN}_{\Sigma-1}^{bp+}$ as the linear combination w of electrode signals. A scalp topography is readily obtained via $a \propto \Sigma w$ where the i^{th} entry of Σw is the covariance between the i^{th} EEG channel and the source that is recovered by w [35, Equation (7)]. Here Σ denotes the subject-specific covariance matrix in the γ -frequency band. A dipole involvement vector g is obtained from a via dynamic statistical parametric mapping (dSPM; with the identity as noise covariance matrix) [36]. The resulting vectors are expected to be in line with previous findings and the hypothesis that the MPC is affected by the SPC.

C. Experimental results

We applied $\text{MERLiN}_{\Sigma-1}^{bp+}$ several times, i.e. with different random initialisations, to the data of each of the 6 sessions.¹⁴ We found that the γ -activation maps a obtained for each spatial filter w were (a) rather smooth and similar to what

¹⁴Since there are only 60 samples per session we decided to select a subset of 33 EEG channels distributed across the scalp (again according to the 10–20 system) after performing the preprocessing according to Algorithm 3. Hence, each time running the algorithm yields a spatial filter $w \in \mathbb{R}^{33 \times 1}$ and a dipole involvement vector $g \in \mathbb{R}^{K \times 1}$.

is typically assumed to be neurophysiologically plausible [37], and (b) consistent across different initialisations within sessions. The dipole involvement vectors are in line with the hypothesis and in five out of six cases identify the MPC as a causal effect of the SPC. The group average and individual results of $\text{MERLiN}_{\Sigma-1}^{bp+}$ are shown in Figure 7.

Group average

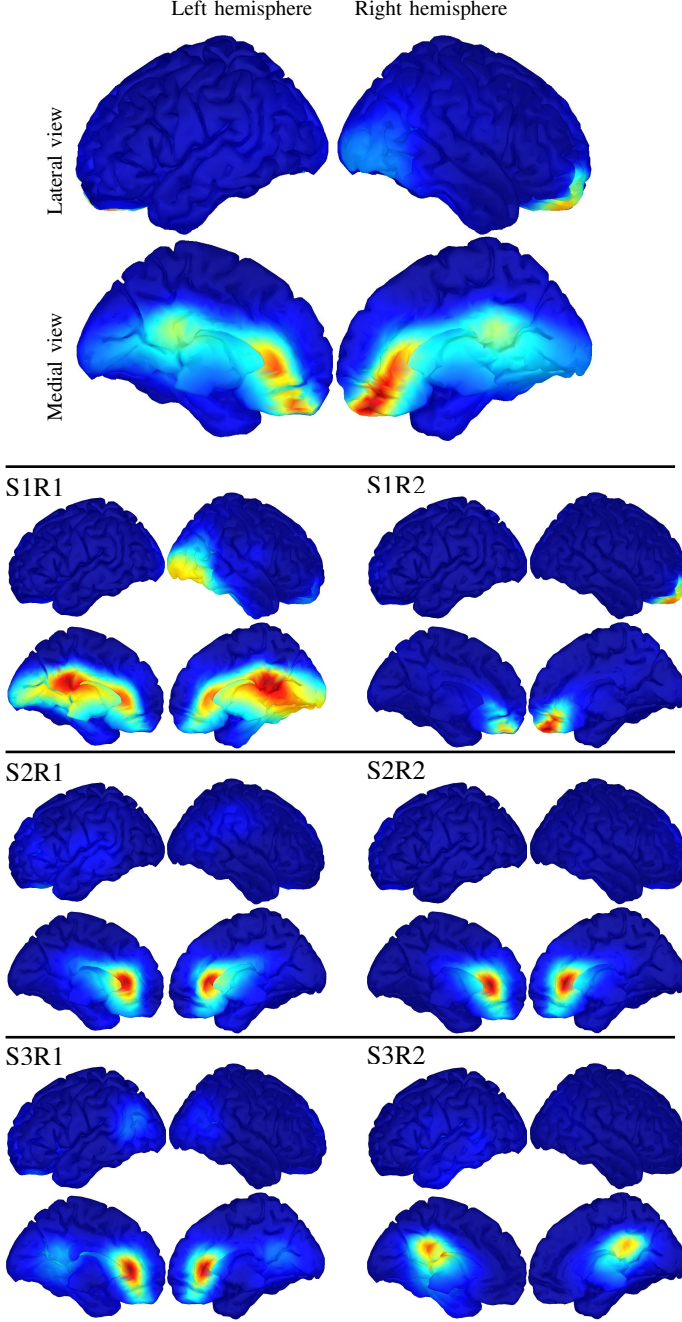


Fig. 7. Dipole involvement for the spatial filters identified by $\text{MERLiN}_{\Sigma-1}^{bp+}$ as group average (first row) and for each session (bottom rows). Each subplot consists of a lateral (top) and medial (bottom) view of the left (left) and right (right) hemisphere. (All colorscales from “blue” to “red” range from 0 to the largest value to be plotted.)

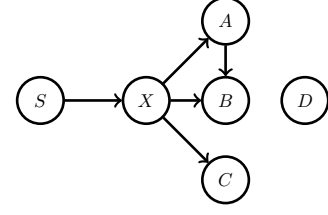


Fig. 8. Example graph.

V. DISCUSSION

While the faithfulness assumption remains untestable one may argue that we are unlikely to encounter violations in practice, e.g. one can show that faithfulness holds almost surely if the causal relationships are linear [38]. Multivariate causal inference methods may be robust against certain violations of faithfulness and hence offer an alternative to such arguments. MERLiN, for example, is able to identify cause-effect relationships in unfaithful scenarios that cannot be revealed by classical univariate approaches. Consider the graph shown in Figure 8 and suppose that the indirect ($X \rightarrow A \rightarrow B$) and direct ($X \rightarrow B$) effects of X on B cancel, i.e. $X \perp\!\!\!\perp B$ wrt. the resulting and unfaithful joint distribution. In this example, univariate methods cannot infer the existence of the edge $X \rightarrow B$ while MERLiN can in principle determine that B is part of the found linear combination and as such directly affected by X .

MERLiN cannot unambiguously recover A, B or C separately as opposed to any linear combination $aA + bB + cC$ that all satisfy the sought-after statistical properties. However, incorporating a priori knowledge as demonstrated in Section II-H can mitigate this ambiguity. It imposes further constraints on the set of vectors that recover variables that while in line with the desired statistical properties are not necessarily causal variables. When analysing EEG data, for instance, one could a priori exclude spatial filters that are neurophysiologically implausible and run optimisation over the complement set instead of the whole unit-sphere.

MERLiN’s fundamental idea is that the construction of causal variables should explicitly take into account statistical properties that correspond to causal structure. This supersedes source separation procedures that often rest on implausible assumptions and are not tailored towards subsequent causal analyses (e.g. ICA in the context of EEG data). Besides MERLiN’s conceptual vantage and good performance both on synthetic and EEG data it is efficient and enabled us to bypass both source localisation (e.g. beamforming, dSPM) and an exhaustive search over 15028 dipoles.

The mentioned link to faithfulness prompts further research on multivariate methods and variants of the faithfulness assumption. Furthermore, it stresses the importance of causal variable construction, a problem in causal inference that often goes unaddressed and is circumvented by presupposing pre-defined meaningful variables.

REFERENCES

- [1] K. Chalupka, P. Perona, and F. Eberhardt, "Visual causal feature learning," in *Proceedings of the 31th Conference on Uncertainty in Artificial Intelligence*.
- [2] P. Nunez and R. Srinivasan, *Electric Fields of the Brain: The Neurophysics of EEG*. Oxford University Press, 2006.
- [3] D. Lowe, "Object recognition from local scale-invariant features," in *Computer Vision, 1999. The Proceedings of the Seventh IEEE International Conference on*, vol. 2, pp. 1150–1157, 1999.
- [4] N. Dalal and B. Triggs, "Histograms of oriented gradients for human detection," in *Computer Vision and Pattern Recognition, 2005. CVPR 2005. IEEE Computer Society Conference on*, vol. 1, pp. 886–893, 2005.
- [5] H. Bay, A. Ess, T. Tuytelaars, and L. V. Gool, "Speeded-up robust features (SURF)," *Computer Vision and Image Understanding*, vol. 110, no. 3, pp. 346–359, 2008.
- [6] A. Hyvärinen and E. Oja, "Independent component analysis: algorithms and applications," *Neural Networks*, vol. 13, no. 4, pp. 411–430, 2000.
- [7] S. Makeig, M. Westerfield, T.-P. Jung, S. Enghoff, J. Townsend, E. Courchesne, and T. J. Sejnowski, "Dynamic brain sources of visual evoked responses," *Science*, vol. 295, no. 5555, pp. 690–694, 2002.
- [8] A. Hyvärinen, J. Karhunen, and E. Oja, *Independent Component Analysis*. Adaptive and Cognitive Dynamic Systems: Signal Processing, Learning, Communications and Control, Wiley, 2004.
- [9] J. Iriarte, E. Urrestarazu, M. Valencia, M. Alegre, A. Malanda, C. Viteri, and J. Artieda, "Independent component analysis as a tool to eliminate artifacts in EEG: A quantitative study," *Journal of clinical neurophysiology*, vol. 20, no. 4, pp. 249–257, 2003.
- [10] A. Delorme, T. Sejnowski, and S. Makeig, "Enhanced detection of artifacts in EEG data using higher-order statistics and independent component analysis," *NeuroImage*, vol. 34, no. 4, pp. 1443–1449, 2007.
- [11] S. Weichwald, T. Meyer, O. Özdenizci, B. Schölkopf, T. Ball, and M. Grosse-Wentrup, "Causal interpretation rules for encoding and decoding models in neuroimaging," *NeuroImage*, vol. 110, pp. 48–59, 2015.
- [12] J. D. Ramsey, S. J. Hanson, C. Hanson, Y. O. Halchenko, R. A. Poldrack, and C. Glymour, "Six problems for causal inference from fMRI," *NeuroImage*, vol. 49, no. 2, pp. 1545–1558, 2010.
- [13] M. Grosse-Wentrup, B. Schölkopf, and J. Hill, "Causal influence of gamma oscillations on the sensorimotor rhythm," *NeuroImage*, vol. 56, no. 2, pp. 837–842, 2011.
- [14] J. D. Ramsey, S. J. Hanson, and C. Glymour, "Multi-subject search correctly identifies causal connections and most causal directions in the DCM models of the smith et al. simulation study," *NeuroImage*, vol. 58, no. 3, pp. 838–848, 2011.
- [15] J. A. Mumford and J. D. Ramsey, "Bayesian networks for fMRI: A primer," *NeuroImage*, vol. 86, pp. 573–582, 2014.
- [16] M. Grosse-Wentrup, D. Janzing, M. Siegel, and B. Schölkopf, "Identification of causal relations in neuroimaging data with latent confounders: An instrumental variable approach," *NeuroImage*, vol. 125, pp. 825–833, 2016.
- [17] M. Eichler and V. Didelez, "On Granger causality and the effect of interventions in time series," *Lifetime Data Analysis*, vol. 16, no. 1, pp. 3–32, 2010.
- [18] J. T. Lizier and M. Prokopenko, "Differentiating information transfer and causal effect," *The European Physical Journal B*, vol. 73, no. 4, pp. 605–615, 2010.
- [19] P. Spirtes, C. Glymour, and R. Scheines, *Causation, Prediction, and Search*. MIT press, 2nd ed., 2000.
- [20] J. Pearl, *Causality: Models, Reasoning and Inference*. Cambridge University Press, 2nd ed., 2009.
- [21] S. L. Lauritzen, *Graphical Models*. Oxford University Press, 1996.
- [22] T. Verma and J. Pearl, "Equivalence and synthesis of causal models," in *Proceedings of the 6th Conference on Uncertainty in Artificial Intelligence*, (Amsterdam, NL), pp. 255–268, Elsevier Science, 1990.
- [23] A. Edelman, T. A. Arias, and S. T. Smith, "The geometry of algorithms with orthogonality constraints," *SIAM Journal on Matrix Analysis and Applications*, vol. 20, no. 2, pp. 303–353, 1998.
- [24] J. Bergstra, O. Breuleux, F. Bastien, P. Lamblin, R. Pascanu, G. Desjardins, J. Turian, D. Warde-Farley, and Y. Bengio, "Theano: A CPU and GPU math expression compiler," in *Proceedings of the Python for Scientific Computing Conference (SciPy)*, June 2010. Oral Presentation.
- [25] F. Bastien, P. Lamblin, R. Pascanu, J. Bergstra, I. J. Goodfellow, A. Bergeron, N. Bouchard, and Y. Bengio, "Theano: New features and speed improvements." Deep Learning and Unsupervised Feature Learning NIPS 2012 Workshop, 2012.
- [26] K. Baba, R. Shibata, and M. Sibuya, "Partial correlation and conditional correlation as measures of conditional independence," *Australian & New Zealand Journal of Statistics*, vol. 46, no. 4, pp. 657–664, 2004.
- [27] P. L. Nunez, R. Srinivasan, A. F. Westdorp, R. S. Wijesinghe, D. M. Tucker, R. B. Silberstein, and P. J. Cadusch, "EEG coherency: I: statistics, reference electrode, volume conduction, laplacians, cortical imaging, and interpretation at multiple scales," *Electroencephalography and Clinical Neurophysiology*, vol. 103, no. 5, pp. 499–515, 1997.
- [28] G. Nolte, O. Bai, L. Wheaton, Z. Mari, S. Vorbach, and M. Hallett, "Identifying true brain interaction from EEG data using the imaginary part of coherency," *Clinical Neurophysiology*, vol. 115, no. 10, pp. 2292–2307, 2004.
- [29] J. Stinstra and M. Peters, "The volume conductor may act as a temporal filter on the ECG and EEG," *Medical and Biological Engineering and Computing*, vol. 36, no. 6, pp. 711–716, 1998.
- [30] S. Li, "Concise formulas for the area and volume of a hyperspherical cap," *Asian Journal of Mathematics and Statistics*, vol. 4, no. 1, pp. 66–70, 2011.
- [31] M. Grosse-Wentrup and B. Schölkopf, "A brain-computer interface based on self-regulation of gamma-oscillations in the superior parietal cortex," *Journal of neural engineering*, vol. 11, no. 5, p. 056015, 2014.
- [32] B. D. Van Veen, W. Van Drongelen, M. Yuchtman, and A. Suzuki, "Localization of brain electrical activity via linearly constrained minimum variance spatial filtering," *Biomedical Engineering, IEEE Transactions on*, vol. 44, no. 9, pp. 867–880, 1997.
- [33] A. C. Chen, D. J. Oathes, C. Chang, T. Bradley, Z.-W. Zhou, L. M. Williams, G. H. Glover, K. Deisseroth, and A. Etkin, "Causal interactions between fronto-parietal central executive and default-mode networks in humans," *Proceedings of the National Academy of Sciences*, vol. 110, no. 49, pp. 19944–19949, 2013.
- [34] J. C. Mosher, R. M. Leahy, and P. S. Lewis, "EEG and MEG: Forward solutions for inverse methods," *Biomedical Engineering, IEEE Transactions on*, vol. 46, no. 3, pp. 245–259, 1999.
- [35] S. Haufe, F. Meinecke, K. Görgen, S. Dähne, J.-D. Haynes, B. Blankertz, and F. Bießmann, "On the interpretation of weight vectors of linear models in multivariate neuroimaging," *NeuroImage*, vol. 87, pp. 96–110, 2014.
- [36] A. M. Dale, A. K. Liu, B. R. Fischl, R. L. Buckner, J. W. Belliveau, J. D. Lewine, and E. Halgren, "Dynamic statistical parametric mapping: Combining fMRI and MEG for high-resolution imaging of cortical activity," *Neuron*, vol. 26, no. 1, pp. 55–67, 2000.
- [37] A. Delorme, J. Palmer, J. Onton, R. Oostenveld, and S. Makeig, "Independent EEG sources are dipolar," *PLoS ONE*, vol. 7, p. e30135, 02 2012.
- [38] C. Meek, "Strong completeness and faithfulness in bayesian networks," in *Proceedings of the 11th Conference on Uncertainty in Artificial Intelligence*, pp. 411–418, 1995.